SANDIA REPORT

SAND2005-6236
Unlimited Release
Printed October 2005

Micro Flame-Based Detector Suite for Universal Gas Sensing

Ron Manginell, Cody Washburn, Matthew Moorman, Tom Hamilton, Rob Manley, James Miller, Patrick Lewis, Paul Clem, Murat Okandan

Prepared by
Sandia National Laboratories
Albuquerque, New Mexico 87185 and Livermore, California 94550

Sandia is a multiprogram laboratory operated by Sandia Corporation,
a Lockheed Martin Company, for the United States Department of Energy's
National Nuclear Security Administration under Contract DE-AC04-94AL85000.

Issued by Sandia National Laboratories, operated for the United States Department of Energy by Sandia Corporation.

Available to DOE and DOE contractors from
U.S. Department of Energy
Office of Scientific and Technical Information
P.O. Box 62
Oak Ridge, TN 37831

Telephone: (865)576-8401
Facsimile: (865)576-5728
E-Mail: reports@adonis.osti.gov
Online ordering: http://www.osti.gov/bridge

Available to the public from
U.S. Department of Commerce
National Technical Information Service
5285 Port Royal Rd
Springfield, VA 22161

Telephone: (800)553-6847
Facsimile: (703)605-6900
E-Mail: orders@ntis.fedworld.gov
Online order: http://www.ntis.gov/help/ordermethods.asp?loc=7-4-0#online

SAND2005-6236
Unlimited Release
Printed November 2005

Micro Flame-Based Detector Suite for Universal Gas Sensing

Ron Manginell, Cody Washburn, Matthew Moorman, Tom Hamilton,
Rob Manley, Greg Shelmadine, and Pat Lewis
Microanalytical Systems Department

Jim Miller, Ceramic Processing and Inorganic Materials Department

Paul Clem, Microsystem Materials Department

Murat Okandan, MEMS Technology Department

Sandia National Laboratories
P.O. Box 5800
Albuquerque, New Mexico 87185-0892

Abstract

A microflame-based detector suit has been developed for sensing of a broad range of chemical analytes. This detector combines calorimetry, flame ionization detection (FID), nitrogen-phosphorous detection (NPD) and flame photometric detection (FPD) modes into one convenient platform based on a microcombustor. The microcombustor consists in a micromachined microhotplate with a catalyst or low-work function material added to its surface. For the NPD mode a low work function material selectively ionizes chemical analytes; for all other modes a supported catalyst such as platinum/alumina is used. The microcombustor design permits rapid, efficient heating of the deposited film at low power. To perform calorimetric detection of analytes, the change in power required to maintain the resistive microhotplate heater at a constant temperature is measured. For FID and NPD modes, electrodes are placed around the microcombustor flame zone and an electrometer circuit measures the production of ions. For FPD, the flame zone is optically interrogated to search for light emission indicative of de-excitation of flame-produced analyte compounds. The calorimetric and FID modes respond generally to all hydrocarbons, while sulfur compounds only alarm in the calorimetric mode, providing speciation. The NPD mode provides 10,000:1 selectivity of nitrogen and phosphorous compounds over hydrocarbons. The FPD can distinguish between sulfur and phosphorous compounds. Importantly all detection modes can be established on one convenient microcombustor platform, in fact the calorimetric, FID and FPD modes can be achieved simultaneously on only one microcombustor. Therefore, it is possible to make a very universal chemical detector array with as little as two microcombustor elements. A demonstration of the performance of the microcombustor in each of the detection modes is provided herein.

Acknowledgments

Many thanks are due to the Sandia LDRD program for funding this work. The authors would like to gratefully thank Doug Adkins, John Anderson, Larry Anderson, Jim Barnett, Nelson Bell, Chris Colburn, Debbie Mowery-Evans, Tim Gardner, Rich Kottenstette, Steve Martin, Curt Mowry, Jacob Richardson, Alex Robinson, James Sanchez, Steve Showalter, Sara Sokolowski, Dan Trudell and Dave Wheeler.

Contents

Nomenclature

DOE	Design Of Experiments or Department Of Energy
FID	Flame Ionization Detector
FPD	Flame Photometric Detector
GC	Gas Chromatograph
HH	Heterogeneous-Homogeneous
LOF	Limit of Flammability
MFC	Mass Flow Controller
NPD	Nitrogen Phosphorous Detector
PMT	Photomultiplier Tube
TID	Thermionic Ionization Detector

1. Introduction

The flame ionization detector (FID) is the most commonly used detector for trace sensing of organic compounds, mainly due to the generality of its response, its excellent signal-to-noise ratio, high sensitivity, and an optimized response that varies little with operational parameters like detector temperature and gas flow rates. [1,2] The conventional FID utilizes an oxy-hydrogen diffusion flame to combust analytes. Ions so produced are collected with electrodes situated around the flame zone and counted using a sensitive electrometer. The FID is commonly referred to as a "carbon counting device" since the magnitude of its response to hydrocarbons is proportional to the number of carbon atoms contained. The equimolar response of the FID to ethane and methane, for example, would differ by a factor of two. Alternatively, 2*n* moles of ethane would give twice the response of *n* moles of ethane. These empirical observations demonstrate the "equal per carbon response" of the FID. The actual ion yield of the FID is of the order of one ion per 10^6 carbon atoms introduced[3].

Though widely used for more than a quarter of a century in analytical chemistry, the exact mechanism of ion production in the flame zone was not completely understood until recently[2]. Via mass spectrometry (MS) it has been understood for quite some time[4,5,6] that ion production from hydrocarbons in flames is primarily the result of chemi-ionization of CHO*:

$$CH + O \rightarrow CHO^* \rightarrow CHO^+ + e^-. \quad (1)$$

The formylium ion, CHO^+, reacts quickly with water produced in the flame to produce hydroxonium ions, the primary charge carrying species responsible for the ultimate FID response[1]:

$$CHO^+ + H_2O = H_3O^+ + CO. \quad (2)$$

It had been assumed that pyrolytic degradation of hydrocarbons in the hot flame zone prior to combustion was responsible for the formation of the formylium ion. The "equal per carbon" rule and the fact that detector response is linear with analyte concentration pointed to pre-combustion analyte degradation to a single, common, one-carbon substance, regardless of the particular analyte used. The exact composition of that common substance, however, was unclear. Through careful experimentation Holm determined that the substance in question is methane: through a variety of reactions, all carbon compounds are ultimately converted to methane in the flame zone[2]. Precombustion degradation, moreover, was shown not to be pyrolytic, but the direct result of reactions with hydrogen atoms which are produced in the hot flame zone[2].

1.1 MicroFID

There is a general trend toward miniaturization of chemical sensors and sensor systems to enable portable use. Zimmerman et. al., was the first to demonstrate how micromachining

can be used to miniaturize the FID.[7,8] As with the conventional FID, a nozzle was used for flame anchoring.[†] The nozzle of Zimmerman's design was, however, micromachined in silicon and glass, and a sample injector/diffuser was integrated into the device. A conventionally-machined cylindrical electrode, approximately 0.5 cm internal diameter and 1 cm tall, was positioned around the flame zone for ion collection. A detection limit of approximately 100 ppb of pentane has been recently demonstrated, requiring typically only 35 mL/min of oxy-hydrogen flow to operate.

The oxy-hydrogen consumption rate of Zimmermann's design is less than a tenth that of the conventional FID, speaking to its improved portability. But the size of the collector used is comparable to that of the conventional FID, primarily due to the fact that although the nozzle was micromachined, the flame produced is still about 2.5 mm in height. Due to physical limitations, it is difficult to further miniaturize this design: stable flames are difficult to achieve on a small scale due to enhanced heat loss arising from large surface-to-volume ratios. To achieve further miniaturization, a different approach is required.

Catalytic materials provide a natural, surface-based method for flame ignition and stabilization. The combination of a microhotplate and catalyst materials for sustained combustion on the microscale is referred to as a microcombustor. (a) (b) (c) (d)
Figure 1 shows a cross-sectional schematic of one of these devices. This design not only permits stable flames in the microdomain, but the limits of flammability (LoF) and usable flow rates are expanded as compared with diffusion flames; combustion temperatures can also be reduced. Other groups have used similar designs to fashion micro chemical reactors for partial oxidation synthesis[9], power generation and hydrogen reforming[10] and gas sensing.[11,12,13,14]

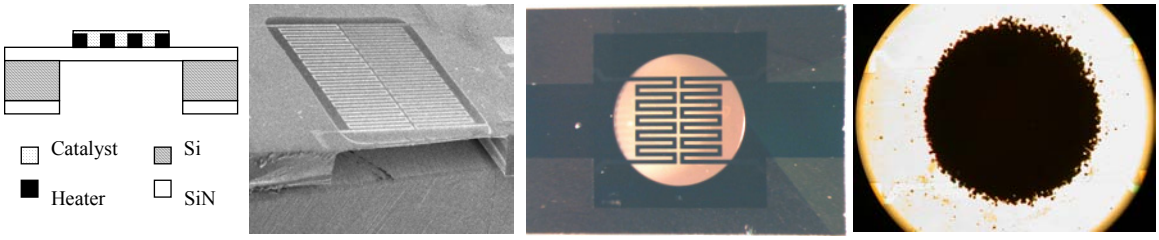

(a) (b) (c) (d)

Figure 1: (a) Cross section schematic of the microcombustor. (b) SEM cross section of the microhotplate, the basis of the microcombustor. (c) An optical photo, backlit of the microhotplate. (d) A spray coated catalyst film on the microhotplate, completing the fabrication of the microcombustor.

[†] The conventional FID design utilizes a sheath of air surrounding a nozzle-generated, centralized jet of hydrogen. In contrast, premixing of oxygen and hydrogen was utilized in Zimmerman's microFID and also in the microFID that is the subject of this correspondence.

By placing electrodes around the flame zone of the microcombustor, a microFID has been constructed and tested[15]. The microFID is the principal subject of this correspondence. Inasmuch as a catalytically-stabilized flame is used instead of a conventional flame, this device is substantially different than the previous work of Zimmermann. The mechanism of ion production is expected to be similar to that given above, but important differences surely exist. The microcombustor can also be used to create a micro nitrogen phosphorous detector (microNPD) and a micro flame photometric detector (microFPD). For the former, the detection electronics are identical to the microFID. Instead of a catalyst, however, a low work function material is used for ionization in the microNPD. Strictly speaking this reaction is not combustion. Instead, high-temperature operation of the microhotplate is used to increase the rate of electron emission from the coating material and thus subsequent analyte ionization. Optical interrogation of the flame zone is used for the microFPD to detect light emission from excited analyte compounds produced in the flame zone. Exploratory efforts into these detection modes will be secondarily described herein. It is critical to note that each of these detection modes, microFID, microNPD, microFPD (as well as calorimetry) can be performed on the same basic microcombustor platform. Since both optical and electronic transduction can be achieved with the same microcombustor, a minimum of two microcombustors is required to achieve simultaneous microFID, microNPD, microFPD and calorimetry: one containing a catalyst for FID/FPD and another containing low work function materials for NPD. To put it another way, it is possible to make a very universal chemical detector array with as little as two microcombustor elements. In practice, a third microcombustor likely would be added to cancel common-mode effects such as ambient temperature or flow variations.

2. Fabrication

The microhotplate, used as a basis for the microcombustor, is fabricated by through-wafer silicon etching. It consists of a silicon nitride membrane suspended from a frame of Si, see Figure 1. Either Bosch etching or KOH etching could be used to release the membrane. In the case of Bosch etching an etch stop layer of 0.5 micron thermally-grown oxide is used to prevent undesired etching of the 1 micron thick low-stress silicon nitride membrane layer; any residual oxide remaining after the Bosch etch is stripped in buffered HF. For KOH etching, no additional etch stop layer is required.
Prior to silicon etching by either method, a thin-film resistive heater is patterned on the membrane layer on the opposite side of the wafer from the etch window. Original embodiments of this device[15] utilized at Ti/Pt metallization, typically ~170 nm of Pt over a 10 nm Ti adhesion layer. The work of Firebaugh[16] and Briand[17], respectively, demonstrated that the use of Ta as an adhesion layer and the passivation of the thin film heater by an overcoat of silicon oxide, silicon nitride, or alternating layers of these materials increases the long-term survivability of the wiring. Recent embodiments of the microcombustor employ such improvements. The dielectric passivation layer currently consists of alternating layers PECVD silicon nitride, and silicon oxide deposited at a stage temperature of 350ºC. Extensive optimization of this film has not been performed, though this stack configuration was the best of the few options studied. Layer thicknesses are, starting with the silicon nitride layer closest to the metal, 100/100/50/50 nm. The order of materials is important since having a source of oxygen in the form of silicon dioxide immediately adjacent to the metallization is undesirable. Alternating the layers is used to compensate the residual stress in the layers, nitride being tensile and oxide being compressive. Finally, adhesion of the deposited catalyst or low-work-function film was superior on oxide surfaces based on nanoindentation and actual device use. Thus the outward facing layer was silicon dioxide to improve adhesion of the active film.

Three main techniques have been used to place the active film (catalyst or low-work-function film) on the microcombustor: drop coating, micropenning and spray coating through a mask. Micropenning is a promising technique for medium to high volume manufacture[15]. But for research quantities of devices, the tubing would often clog between occasional uses of the system. All microcombustors produced recently for calorimetry, microFID and microFPD rely on spray coating through a mask. This technique works well for research quantities of devices as there is minimal tubing to be clogged, but this technique appears to be scalable to large volumes of devices. Platforms for microNPD have been drop coated[†], though they could be spray coated as well. The spray coating system consists of a computer-controlled robotic stage to allow coating of numerous devices at once and to allow for thickness control through the application of many thin coating layers in multiple passes. The stage is heated to a constant 160°C to control solvent removal from the deposited film. See Figure 2 for images of the spray-coating system. Controlled drying is important for preventing mud-cracking of the film and controlling film thickness uniformity. Following

[†] The microNPD uses a microhotplate platform, but it is important to emphasize that the NPD does not rely on combustion for ionization; the microcombustor microhotplate increases the rate of electron production from the low-work-function coating.

deposition, the devices were placed in a vacuum oven for 12 hours at 60 °C to ensure the removal of all liquid before device operation. Catalyst films deposited were 10% platinum in alumina, the details of preparation being provided in reference 15. The low work function films were produced by sol gel techniques and employed materials like rubidium and cesium.

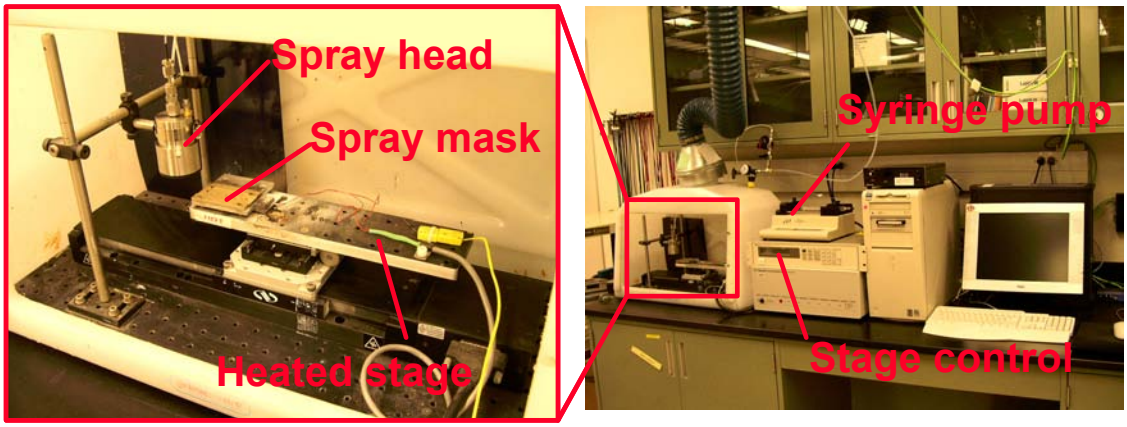

Figure 2: The computer-controlled spray coating system. Several microcombusters are coated at once by placing them under the spray mask together.

3. Fixture and Device Design

To provide gas flows to the microcombustor a variety of test fixtures have been designed, implemented, tested and improved upon throughout this program. Reference 15 describes several such fixtures, including that used in the critical first demonstration of the microFID. To be convinced that the microFID was functioning properly without the potentially confounding influence of custom electronics, a Varian GC/FID system was modified according to Figure 3 and tested. This embodiment permitted several operational parameters to be investigated quickly using the Varian electronics for detection and bias. Importantly, the hydrogen flow rate was reduced to ensure combustion on the microcombustor and not flame-anchoring on the Varian nozzle/jet. There is insufficient space here to describe the details of these experiments, but suffice it to say that this embodiment was used to verify the behavior of the microFID over a broad range of operational parameters using well-characterized commercial electronics.

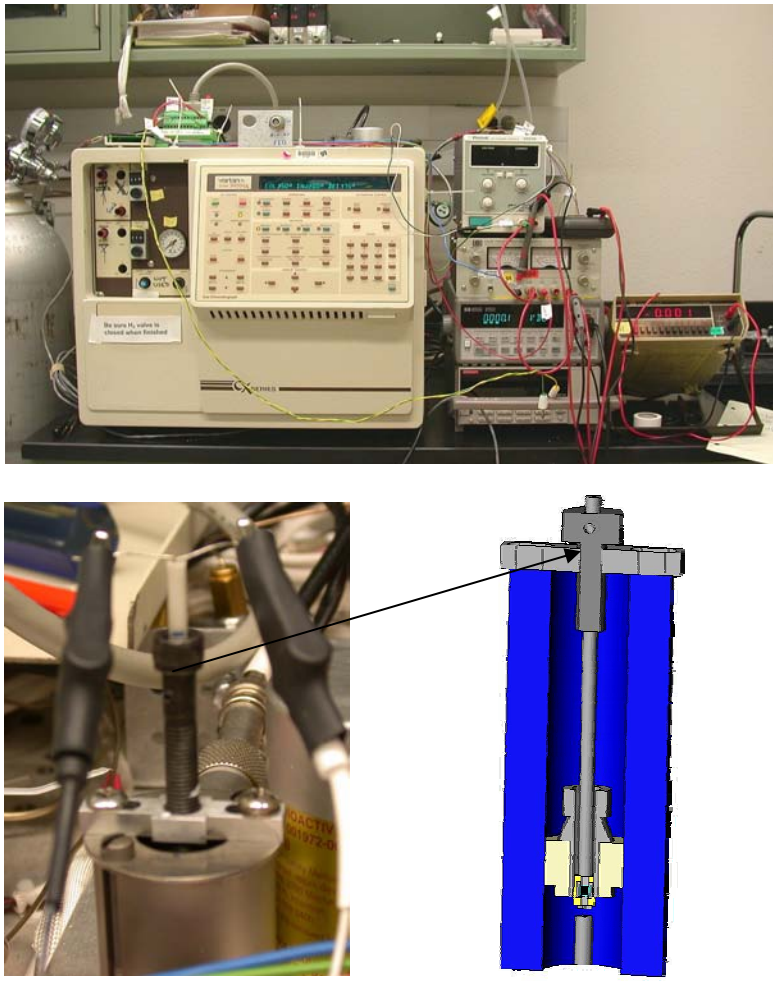

Figure 3: At top is the modified Varian 3400 GC/FID system that employs the modifications shown at the bottom of the figure. A custom adapter allows the microcombustor to be installed near the collector of the Varian FID.

The latest fixture is shown in Figure 4. A clamshell structure with an o-ring seal is used to provide a gas-tight seal around the active area of the microcombustor and to compress pogo-pin electrical connections to the device. As shown in the schematic section of this figure, the active film is placed on the reverse side of the membrane (the etch well side of the device, in contrast with what is shown in Figure 1). A stainless-steel electrode is fixed in the lid for ion collection and is spaced approximately 0.5 mm from the microcombustor surface. The biasing and collection scheme is indicated in Figure 5. The potential difference between the collector and the hotplate is established by the combination of a supply, biased above ground from 25 – 200V, and the hotplate heater potential, usually 5 – 15 V. For 25V bias and 10 V heater potential, the average field in the gap is therefore 300 V/cm.

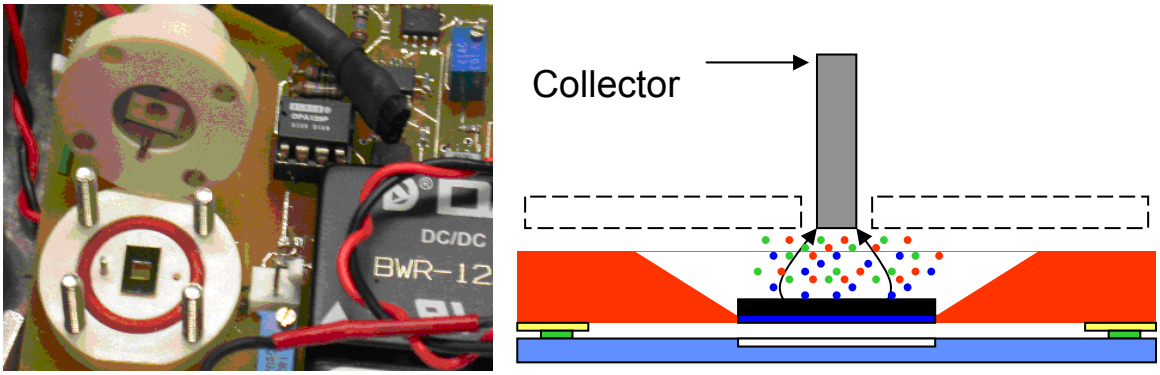

Figure 4: A photograph and schematic of the new clamshell microcombustor fixture. At left the lid of the fixture is propped open to show the microcombustor in the base and the circular collector in the lid.

It is not necessary to have the electrode in the lid as in Figure 4, though this design is very convenient, easy to implement and is in fact used in the bulk of the discussions below. Nonetheless, an important advantage of micromachining a microFID is that ability to (a) incorporate thin-film electrodes on chip and (b) monolithically-integrate detection and control electronics with the electrodes. Neither of these can be achieved by conventional FID, and, given the presence of deleterious parasitic influences in macroscale systems, there is expected to be an advantage to on-chip electronics. This is analogous to the improvements in micromachined accelerometers where monolithic electronics eliminate parasitic off-chip interferences. To the best of the knowledge of the authors Figure 6 shows the first implementation of integrated, on-chip electrodes with a microFID. Data taken with this device, shown in Figure 7 illustrates operation but points to the need for automated injection to remove variability introduced by the use of syringe injections as was done here. This issue is addressed below. The first-ever incorporation of front-end preamplification with fringe-field electrodes on chip is illustrated in Figure 8. Using a picoamp current source, the functioning of the NMOS differential pair preamplifier was verified. The next step in this development is to apply the active film to the surface and test operation during analyte combustion. As aforementioned, most data has actually been taken with the design of Figure 4, not using the on-chip electrodes or electronics. Now that the functioning of

this, simpler configuration is now fairly well understood, it is now feasible to return to the monolithic design to explore fully its operation.

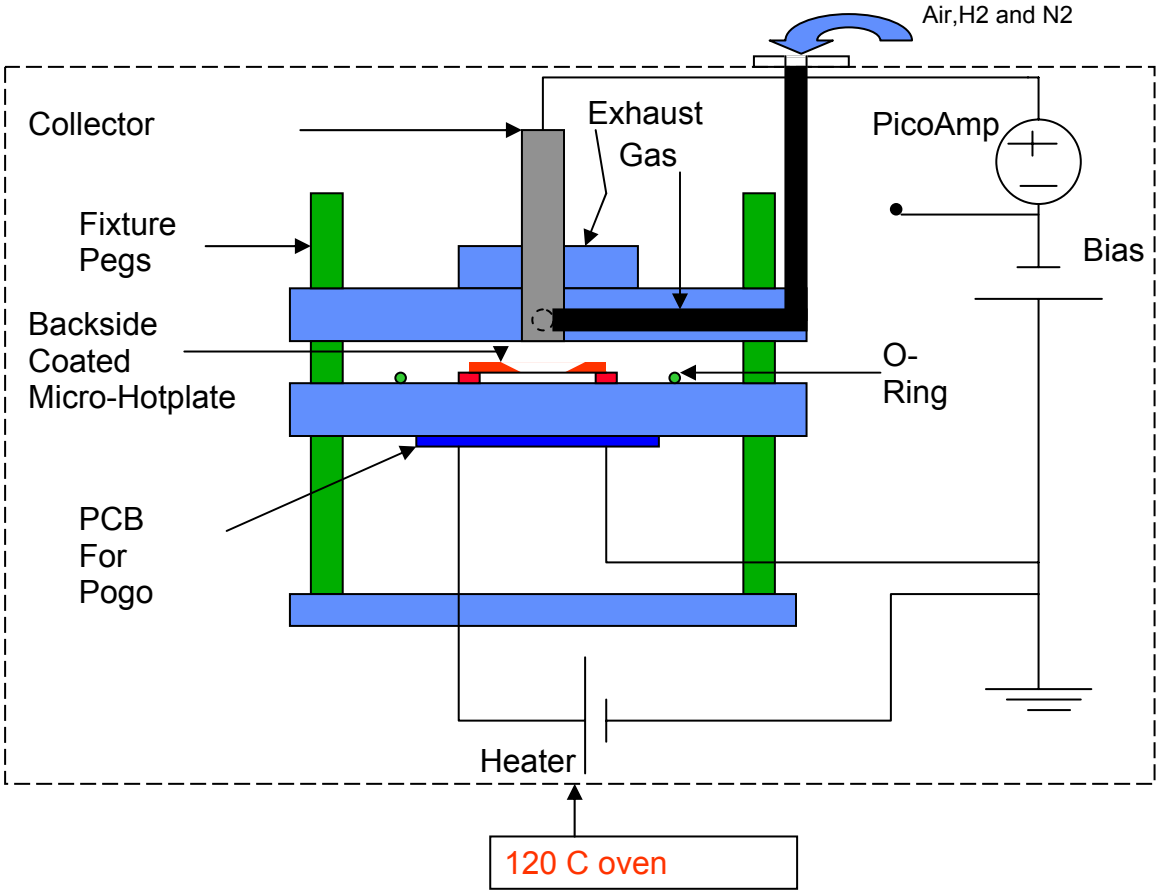

Figure 5: Schematic of the clamshell microFID/NPD fixture.

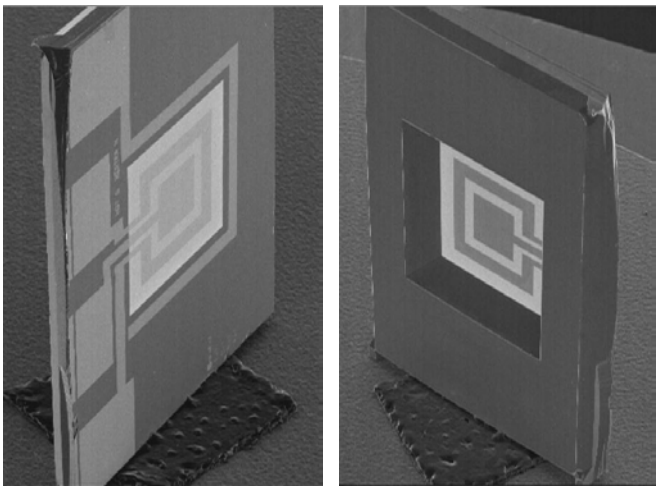

Figure 6: The front (left) and back (right) of the microFID with on-chip bias and collection electrodes.

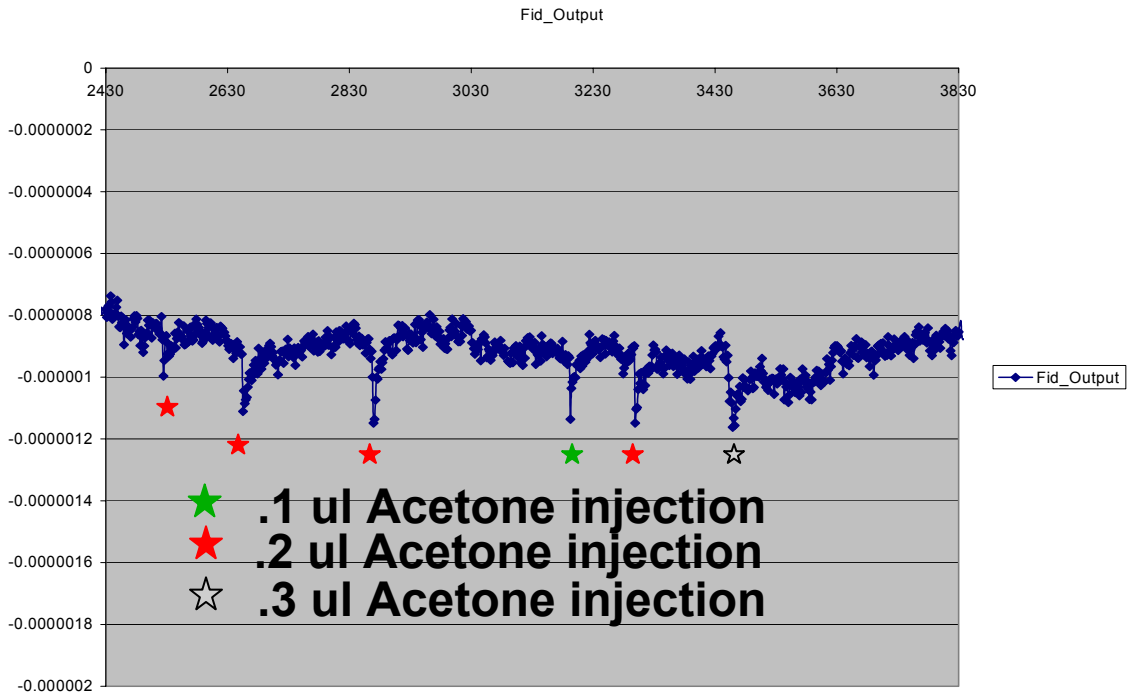

Figure 7: MicroFID response with the on chip electrodes.

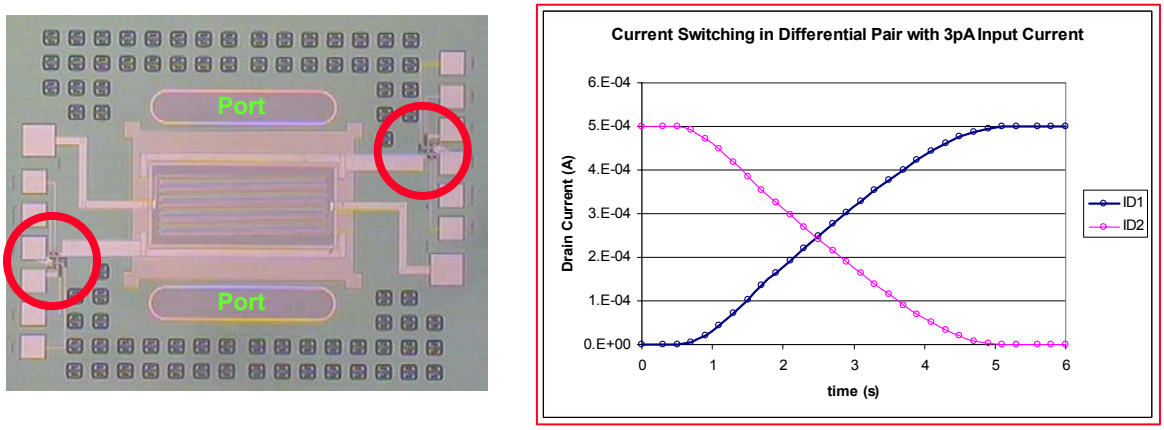

Figure 8: Left: photo of the microFID with on-chip electrodes surrounding the rectangular microcombustor platform and attached to NMOS differential pair amplifiers. Right: response of the NMOS amplifier to 3 pA of input current.

4. Test System

For calorimetry, the effective change in resistance of the heater during combustion of analytes is measured. This can be achieved using a constant-temperature control circuit, which has the benefit of preventing unwanted variations in microcombustor temperature during sensing.[15,18] Of course, constant voltage or constant current operation can also be used, and in these cases current or voltage, respectively, is measured as a gauge of the heat liberated by analyte combustion on the device. In any case, for calorimetric detection a circuit is used to measure the effective change in resistance of the microcombustor heater. For microFID or microNPD, the electrode and electrometer system mentioned above is required. For the microFPD, an optical detector is required. A fiber optic can connect a suitable optical detector to the combustion zone, or direct interrogation can be used, provided an intermediate heat shield is used as well. The optical detector is typically a photomultiplier tube (PMT) but an avalanche photodiode is also possible. Details are provided next.

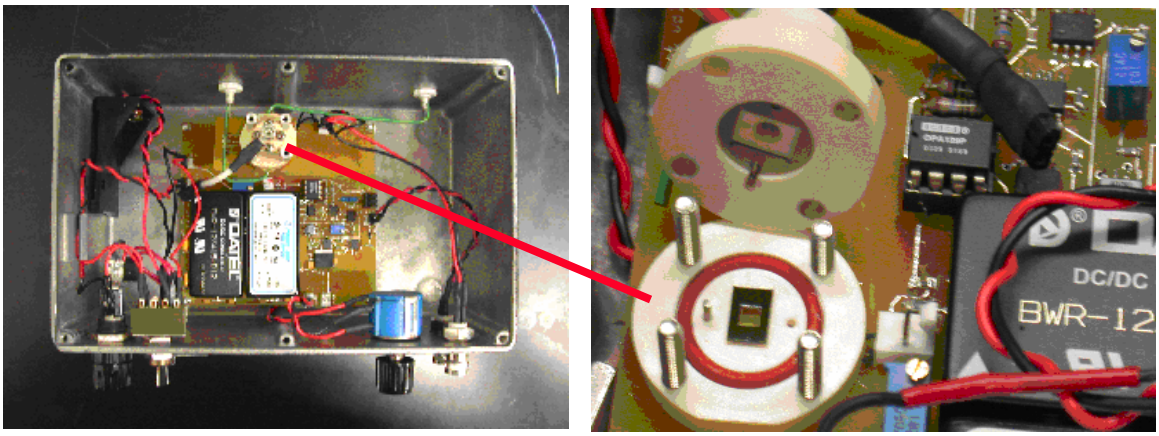

Figure 9: Left: portable field box, slightly larger than a brick, for the microcombustor sensor. Right: the clamshell fixture opened to view the device.

The fixture of Figure 4 has been incorporated into automated data acquisition/control systems and can test microFID, microNPD and calorimetric response to analytes. At the heart of the system is a portable box, Figure 9, containing at present the fixture, a fixture heater to prevent water condensation with the FID mode, and a sensitive custom electrometer. The box is configured to incorporate independent heater controllers for the fixture and microcombustor heater, though for testing below, external supplies were used. The box is also enabled for a miniature pump and valve system to introduce samples through a microGC connected to the microFID. While initial microNPD testing utilized these amenities, initial microFID testing did not; instead a conventional GC inserted into an oven was used instead to simplify matters, as shown in Figure 10, Figure 11 and Figure 12. Data acquisition was accomplished using a laptop connected through a National Instruments BNC2120 board. Mass flow controllers were calibrated using a Sensidyne Gilibrator 2, true volumetric flow meter and were controlled using a Brooks model 0154 controller. MFCs

controlled hydrogen, air and nitrogen GC carrier flow. When a syringe and sample injector was not used, sample introduction was automated using a VICI 6-way valve (Valco, Houston, TX) and 100 microliter sample loop.

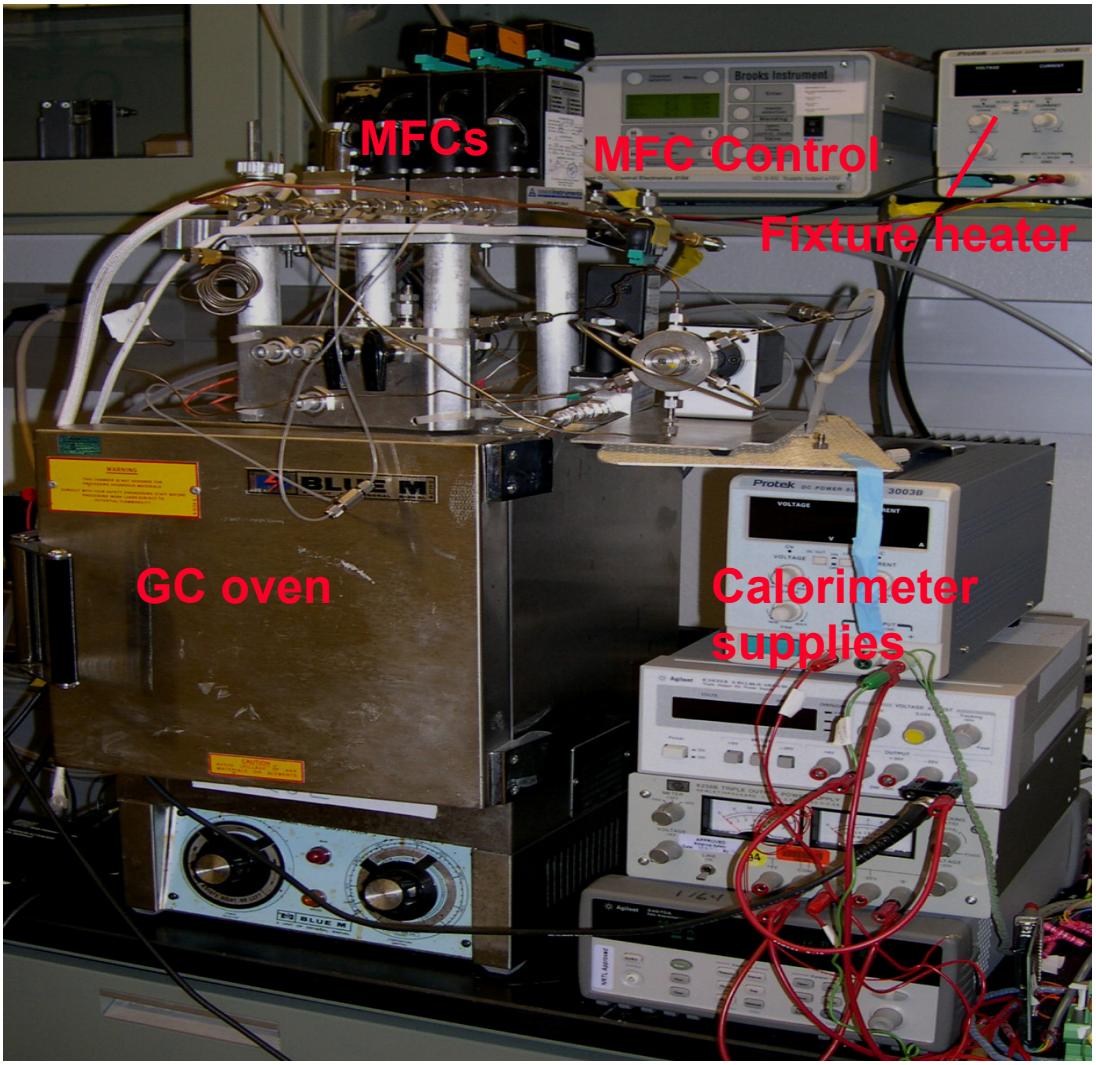

Figure 10: MicroFID and calorimeter apparatus, view from the right.

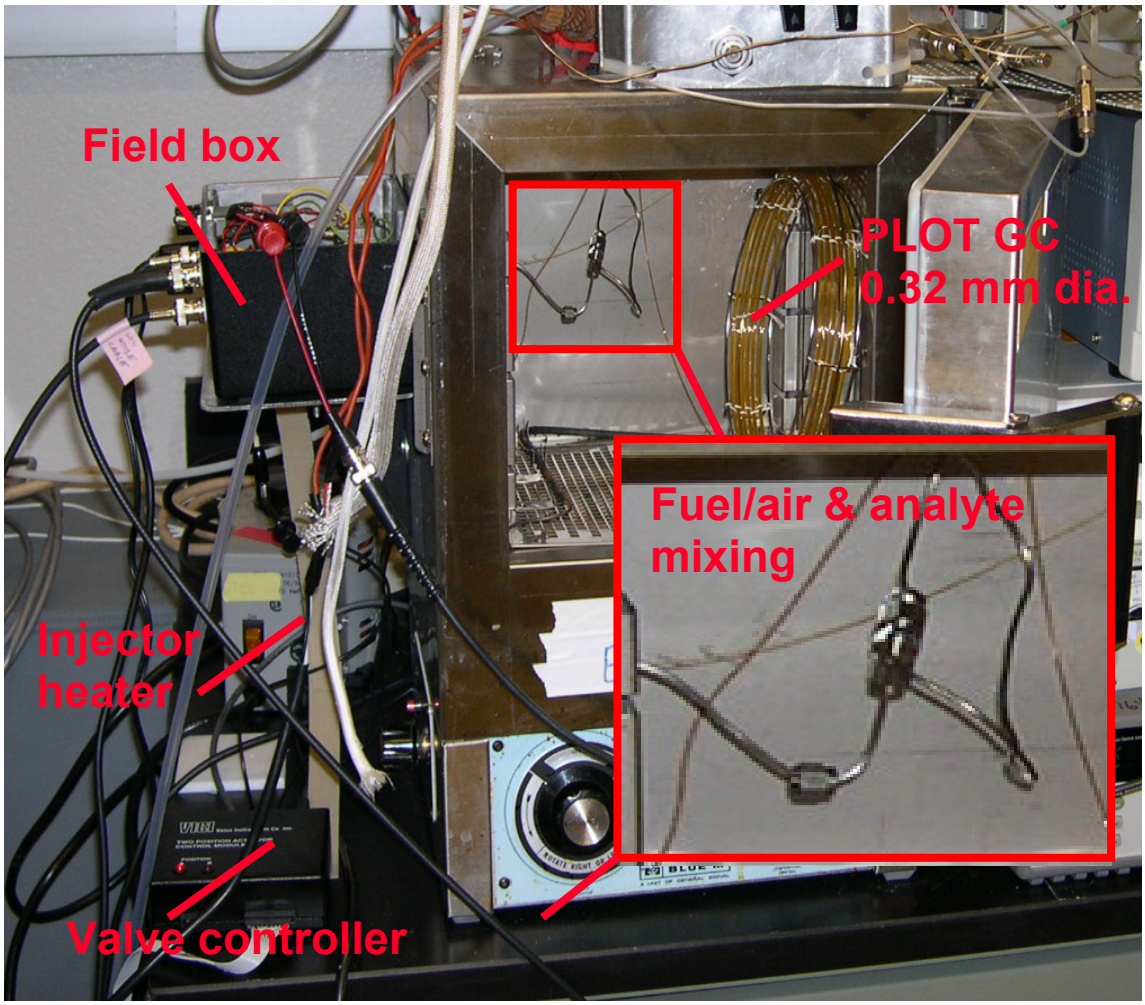

Figure 11: View of the microFID apparatus from the left with oven door open to reveal the GC and mixing tee. The field box of Figure 9 is mounted on the oven to easily take advantage of the heated PLOT GC.

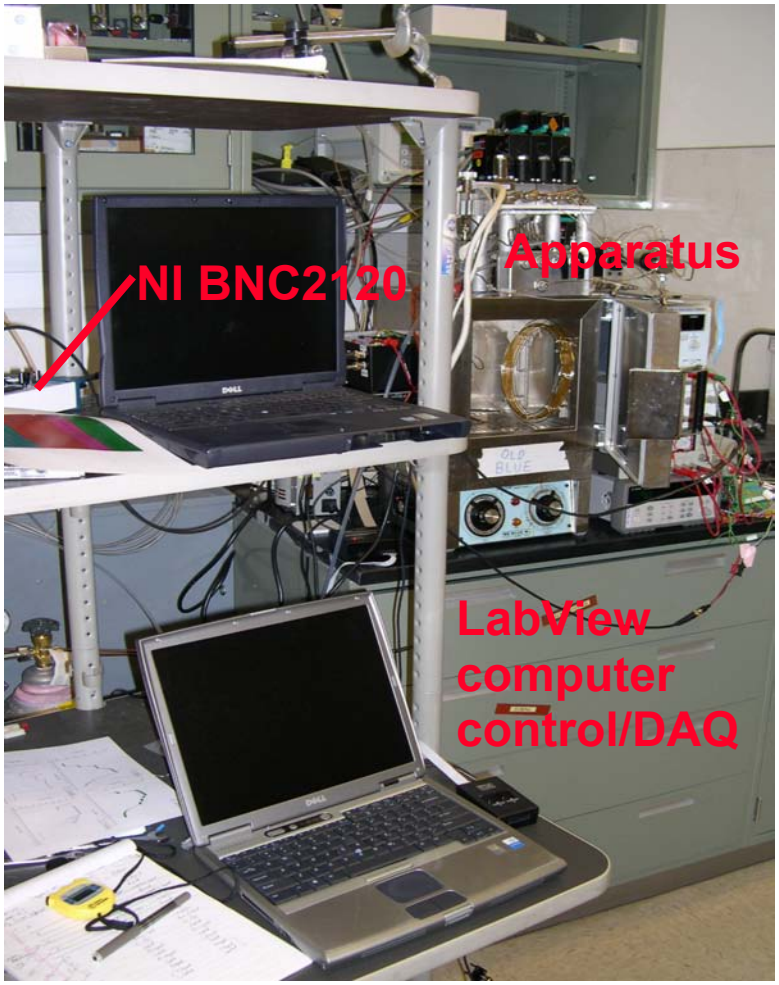

Figure 12: View of the test system from the far left showing the data acquisition (DAQ) and computer control.

To test the microFPD, the fixture of Figure 4 was slightly modified to allow introduction of an optical fiber (220 – 1150 nm), as shown in Figure 13. Using an Ocean Optics inline filter holder (Model FHS-UV), either a 394 nm or 525 nm notch filter (+/- 10 nm pass band width, Edmund Scientific) was used to detect sulfur or phosphorous, respectively. The output of the filter holder was coupled to a detector. For most tests a light-shielded Hamamatsu ultraminiature PMT (Model H5784) was used. For a limited number of tests a Geiger photodiode was used. Direct coupling of the optical detector with a heat shield and filter can be accomplished with this fixture, but for ease of demonstration, the optical fiber approach was taken at first. Signal-to-noise is expected to improve when the intermediate fiber is removed.

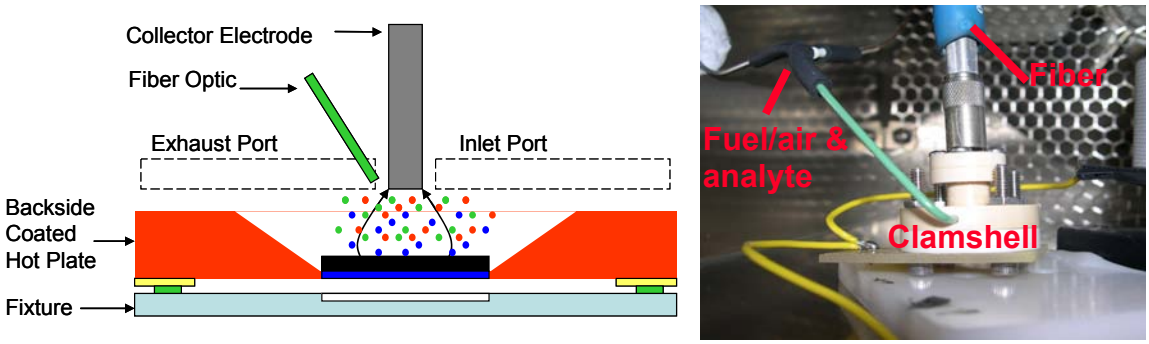

Figure 13: Left, schematic of the microFPD modifications. Right, the actual fixture placed in a Varian GC oven.

5. Calorimetry

As aforementioned for calorimetry, the effective change in resistance of the heater during combustion of analytes is measured. A constant-temperature control circuit that can be used for this purpose is shown in Figure 14. In this circuit the amplifier circuits at left measure the proportional voltage and proportional current through the microcombustor. Using the AD633 and its attendant circuitry, the proportional resistance is obtained and is compared with a reference, or set point, using the comparator represented by the amplifier circuit at the right side of the figure. The output of the comparator controls the gate of the FET, far right in the figure, and therefore the current through the microcombustor. Via this circuit, the power to the device required to maintain constant resistance (or temperature, via the temperature coefficient of resistance of the thin-film heater) is obtained. Exposure of the device to natural gas/air is shown in Figure 15. The baseline in air is stable. During periodic introductions of fuel air of various concentrations the power required to maintain the device at 400ºC drops, as combustion on the device provides the balance of power. This data was taken in a clamshell fixture very similar to that in Figure 4, but not exactly the same.

An advantage to catalytically-supported combustion over traditional diffusion flames is that the limits of flammability (LoF) are expanded. See Table 1. Reference 15 illustrates this clearly even though the final limits of these hydrocarbons have not been reached in these tests. Other calorimetry data is given below, in conjunction with microFID and microNPD response.

Table 1: Comparison of conventional and unoptimized catalytic combustion

Hydrocarbon	Conventional Limits of Flammability	Catalytically-Stabilized Limits of Flammability
Natural Gas	4-16%	1.3-35.5%
Methane	5-15%	2-20%
Ethane	2.9-13%	1-4%*
Propane	2.1-9.5%	1-11.5%

*Ethane has not yet been tested beyond the upper limit of flammability.

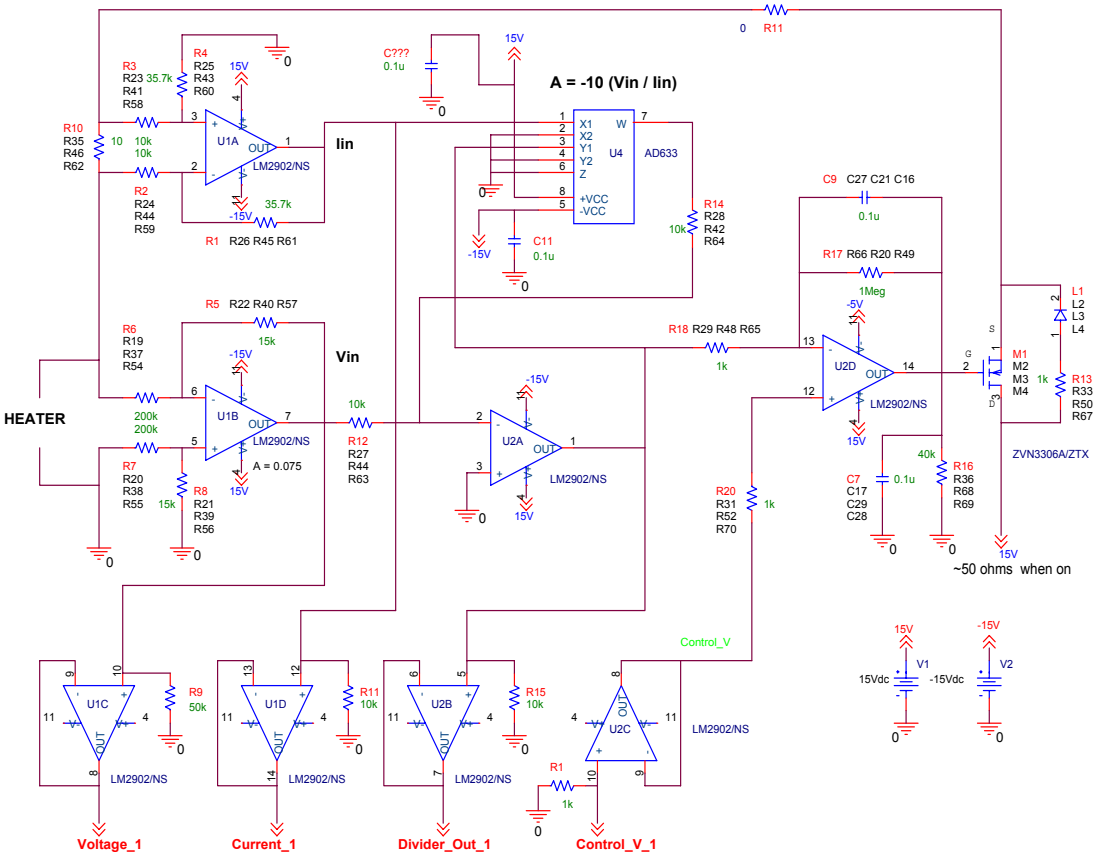

Figure 14: Constant resistance (temperature) control circuit used for calorimetry. The microcombustor heater is placed at the location called “heater”.

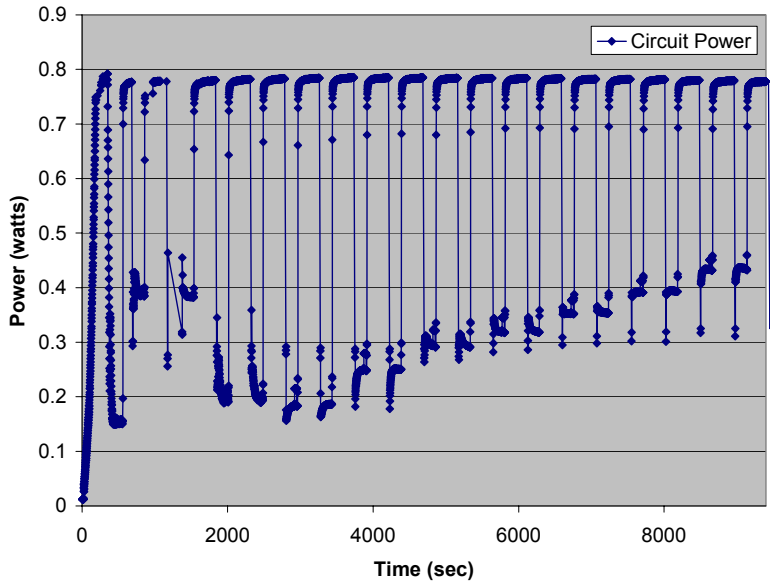

Figure 15: The power provided to the microcombustor as a function of time during periodic exposure to natural gas/air mixtures. The baseline is taken in air. When natural gas is introduced, combustion provides the balance of power required for constant temperature.

6. FID

The test system of Figure 5, Figure 9, Figure 10, Figure 11, and Figure 12 was used for the data given in this section. Where noted, a syringe and sample injector was used instead of the sample valve. The basic response of the system to methane, ethane and propane is shown in Figure 16 for oxyhydrogen flow of 36.3 mL/min. The methane baseline, though drifting due to the lack of proper burn in before testing, still provides adequate signal/noise for a 20 microliter injection of methane. The response for ethane and propane was taken subsequent to the methane data and has a much more stable baseline, showing the necessity of proper conditioning of the active microcombustor film, achieved in this case through the preceding methane data series. Note, given equal-carbon response, the lower limit of detectability of the microFID for higher carbon-number hydrocarbons is expected to be superior to the results shown here.

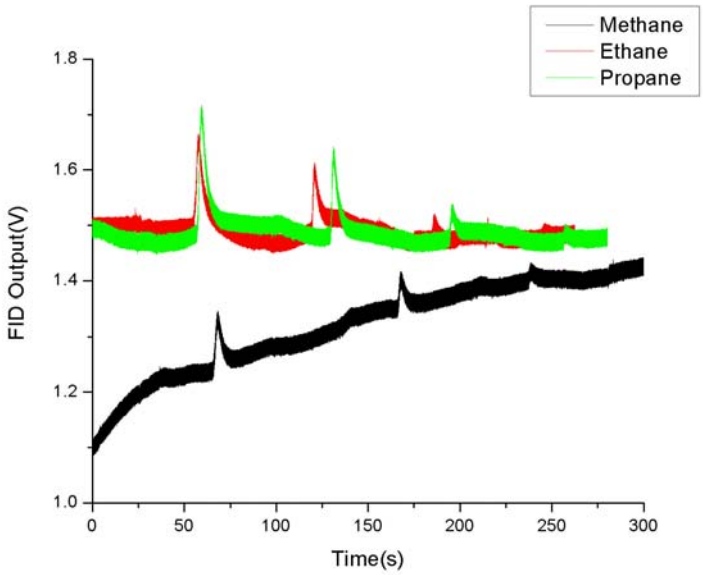

Figure 16: MicroFID responses to 100, 50, 20 and 10 microliter syringe injections of methane, ethane and propane. The methane series was taken first and shows drift due to device conditioning. Hydrogen, air and nitrogen carrier flows were, respectively, 14.5, 21.8 and 15.1 mL/min.

To gain an appreciation for the effect of bias voltage on microFID response, Figure 17 plots bare response against ethane versus bias. Peak height versus bias, abstracted from this data, is plotted in Figure 18. The current-voltage characteristic is more similar to that of reference 19 than that of reference 8. The latter bears a resemblance to the I-V curve of a non-sustained plasma, at least the low voltage portion where there is a transition from the recombination regime to the saturation regime. The former, like the data of Figure 18, shows approximately Ohmic response.

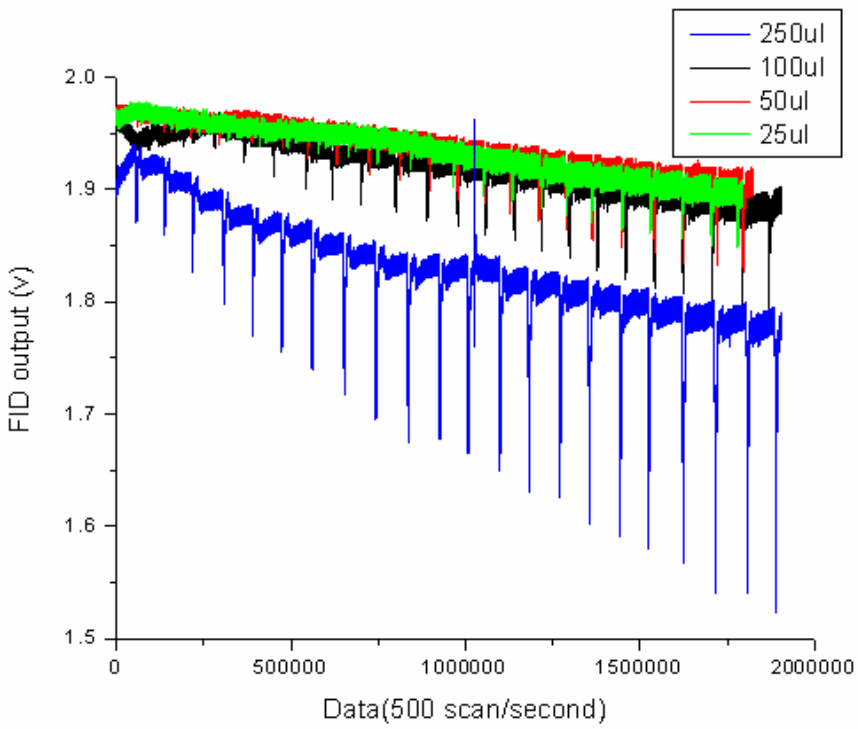

Figure 17: MicroFID responses to various syringe injection volumes of ethane as a function of bias voltage. Hydrogen, air and nitrogen carrier flows were, respectively, 9.3, 37.8 and 5.1 mL/min.

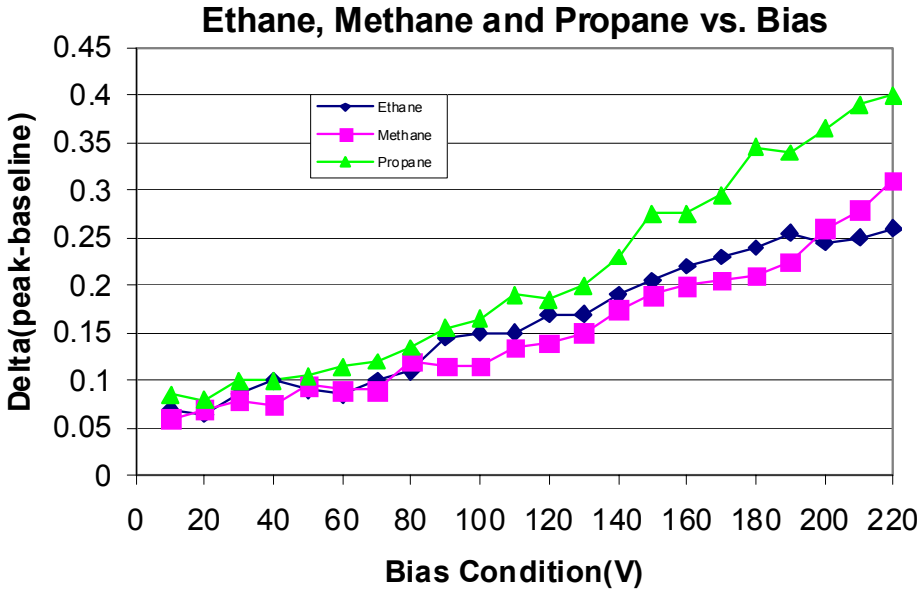

Figure 18: MicroFID peak height as a function of bias voltage. Hydrogen, air and nitrogen carrier flows were, respectively, 9.3, 37.8 and 5.1 mL/min.

There are numerous design and operational parameters for the microFID. These include electrode design and spacing, total bias, catalyst composition and operation temperature. Gas flow rates, namely, hydrogen, air, nitrogen carrier, and total flow rate, are also critical. In order to study these effects, a statistical design of experiments (DOE) was undertaken. Based on initial scoping experiments, suitable operational ranges on bias and gas flow were determined. The simplest electrode design, the pseudo parallel plate configuration of Figure 4, was chosen with a fixed gap of 0.5 mm and a fixed bias of 100V. The catalyst composition was 10% platinum in alumina and the operation temperature were fixed at 450°C. The three design parameters were hydrogen, air and nitrogen carrier flow rate using a Box-Behnken DOE. Fixed-volume injections of 100 microliter of ethane were used and the resulting peak height from baseline was taken as the microFID response.

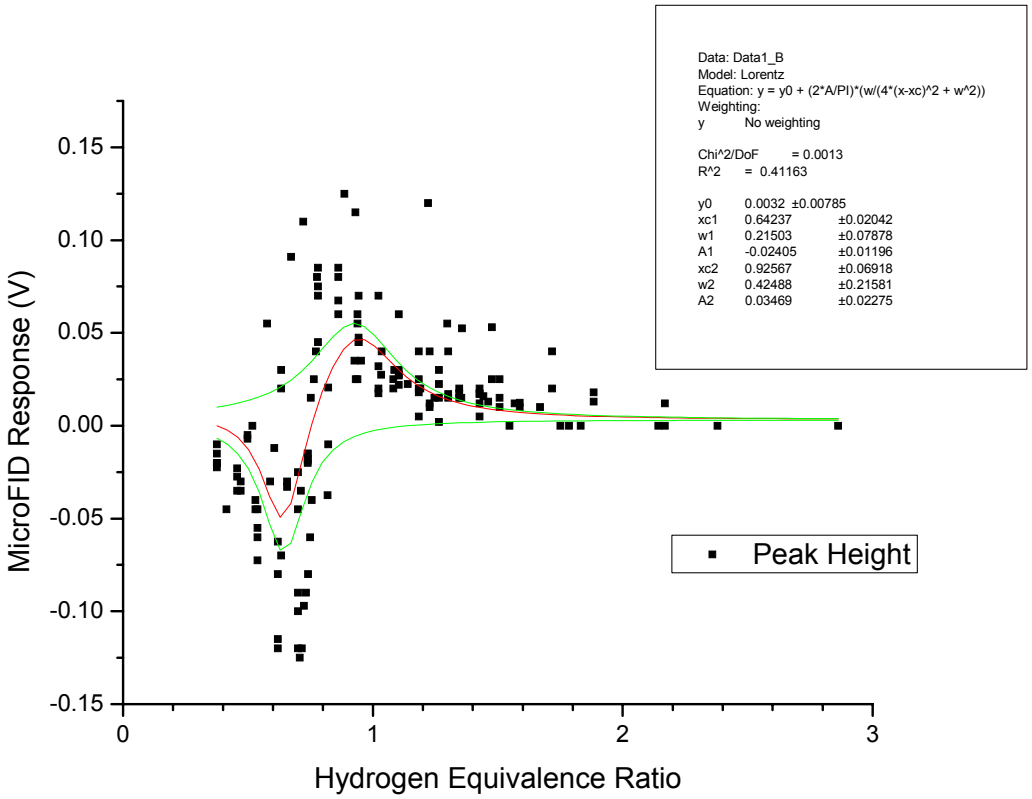

Figure 19: MicroFID DOE Results. Two Lorentz peak fits and a composite fit are used to guide the eye.

All the results of the microFID DOE are given in Figure 20 plotted against the hydrogen/air equivalence ratio for ease of comparison with the literature. Equivalence ratio (Φ) normalizes the actual fuel/air ratio to the stoichiometric fuel/air ratio[†], and therefore has a value of unity for stoichiometric mixes. Lean mixtures reside in the range of $\Phi < 1$, while

[†] For hydrogen-air combustion, 34.3 grams of air is required for stoichiometric combustion of 1 gram of hydrogen, assuming 21% of air is oxygen.

rich mixtures are characterized by $\Phi > 1$. It is important to note that in the plots, only the hydrogen/air equivalence ratio is described and the effect of hydrocarbon analyte introduction to the fuel/air mix is not included in the equivalence ratio calculation. The addition of hydrocarbon analytes would have the effect of shifting the combustible mixture towards the fuel-rich regime.

The data shows two peaks, one positive at about $\Phi \sim 1$ and one negative at roughly $\Phi \sim 0.6$, with a transition through zero at $\Phi \sim 0.8$. At this point in time the nature of the response data is not completely understood. The traditional FID response does not, to the author's knowledge, display such a bipolar response. However, traditional FID is usually operated under extremely lean conditions, typically 10% hydrogen in air. This is at the far left of the equivalence range tested herein and shown above, so direct comparison is difficult. Nonetheless, is seems likely that the mechanism of ion generation in the microFID is complicated by the details of the catalysis reaction. This is discussed next.

Flame temperatures in the microcombustor of Norton et. al. have been observed to increase as stoichiometry is approached.[20] Futhermore, Norton showed that equivalence ratios exceeding 0.6 yield homogeneous/heterogeneous (HH) combustion, a situation were both surface catalytic combustion and homogeneous gas phase combustion occur simultaneously. As mentioned above, ethane injection peaks increase the instantaneous equivalence ratio seen by the microcombustor, effectively shifting the data results towards more fuel rich mixtures. Therefore, the transition to HH combustion in the microFID with burning analyte can be expected to occur at slightly higher than $\Phi = 0.6$, closer to $\Phi = 0.8$ where the zero crossing is seen in the data. Increased flame temperature and HH combustion could collectively explain the increase in response near equivalence. Production of hydrogen radicals likely would be enhanced under these circumstances, accelerating the rate of hydrocarbon cracking and ion production according to the theory of operation of the FID described previously. As the equivalence ratio was further increased in this data, the flow rate also increased, making it possible for ions to be swept out of the fixture before collection. This can explain the decrease in signal at increased equivalence.

In the range of $0.2 < \Phi < 0.8$, the microFID response swings negative. It has been shown that multiple steady states exist in the range of $0.3 < \Phi < 0.55$ for Norton's microcombustor, depending on the startup history. In other words, flame temperature hysteresis exists dependent on equivalence ratio, and in this range both heterogeneous and homogeneous combustion can take place depending on the direction of approach to this domain. The lower branch of said hysteresis curve, starting at $\Phi = 0$ and proceeding to $\Phi = 0.5$ on the ascent with increasing equivalence ratio is characterized by catalytic, heterogeneous reactions. The upper branch is HH combustion. Ethane injections in the microFID again would tend to shift the equivalence range, possibly allowing hysteresis up to $\Phi = 0.8$, and would tend to approach higher equivalence from below, remaining on the catalytic branch. It seems that the nature of ion generation in this domain is different than the traditional FID, perhaps because of influence of catalytic reactions. Radical quenching is known to occur with catalytic combustion, possibly modifying the ion production mechanism. Also, the location of ion generation is likely to be closer to the catalyst surface (farther from the collection electrode), influencing the microFID response. At very lean conditions, ethane

and hydrogen combustion can extinguish, leading to the fall off in signal at low equivalence ratios.

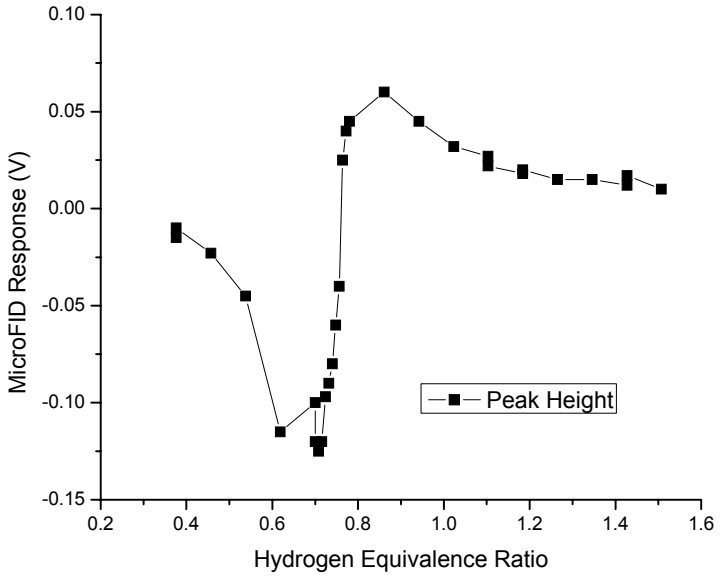

Figure 20: MicroFID response for constant air and nitrogen flow. The solid lines are meant to guide the eye.

Noise in the data of Figure 19 seems to arise from minor flow variations. Thus the data of Figure 20 was taken for constant air and nitrogen flow. Hydrogen flow was varied to effect a change in equivalence ratio. The same basic behavior is observed. To understand the nature of the response additional experiments were conducted. First, the operation of the electrometer with positive and negative inputs was verified. Positive current inputs from a Keithly 220 precision source to the electrometer yielded negative going deviations from baseline on the electrometer. Negative current inputs from a Keithly 220 to the electrometer yielded positive going deviations from baseline. Thus, both positive and negative going peaks are physically possible. To be sure that gas-phase electrochemistry was not the culprit, we verified that there was no interaction between the hotplate circuit and the electrometer circuit. Current swings on one were not reproduced in the other. The lack of microFID response to ethane injections without the hotplate on showed that ethane thermal conductivity was not influencing the system response. Furthermore, the total flow rate of inert gases does not influence the microFID response. The flow rate of hydrogen does influence the baseline level, peaking near equivalence ratio of 0.7. Finally, the temperature of the catalyst seems to increase the background noise, as expected. Future experiments are aimed at further understanding the overall nature of the microFID response.

7. NPD

The nitrogen-phosphorous detector is in a class of detectors known as thermionic ionization detectors (TID). This designation refers to the fact that analytes are ionized through interaction with a heated surface containing a low work function material. For conventional NPD the material is typically a composite of rubidium and alumina or cesium in alumina. For the microNPD of this work a sol gel containing these materials was produced by standard techniques, drop coated on the microhotplate and cured at 400°C in nitrogen. During operation, microNPD is situated in the fixture of Figure 4, the microhotplate is held at a temperature of 600°C and the electronics of the handheld box shown in Figure 9 is used for ion detection. Analytes injected into the system pass by the hot microNPD surface and are ionized depending on their exact nature. Nitrogen and phosphorous compounds form electronegative radicals in the thermochemical boundary layer and readily extract an electron from the low-work function surface, becoming ionized. Ordinary hydrocarbons, on the other hand, do not form compounds that are highly electronegative and are only weakly ionized. Based on this mechanism, therefore, the selectivity of the NPD is 10,000:1 for detecting N and P compounds compared with ordinary hydrocarbons. This effect is illustrated in Figure 21.

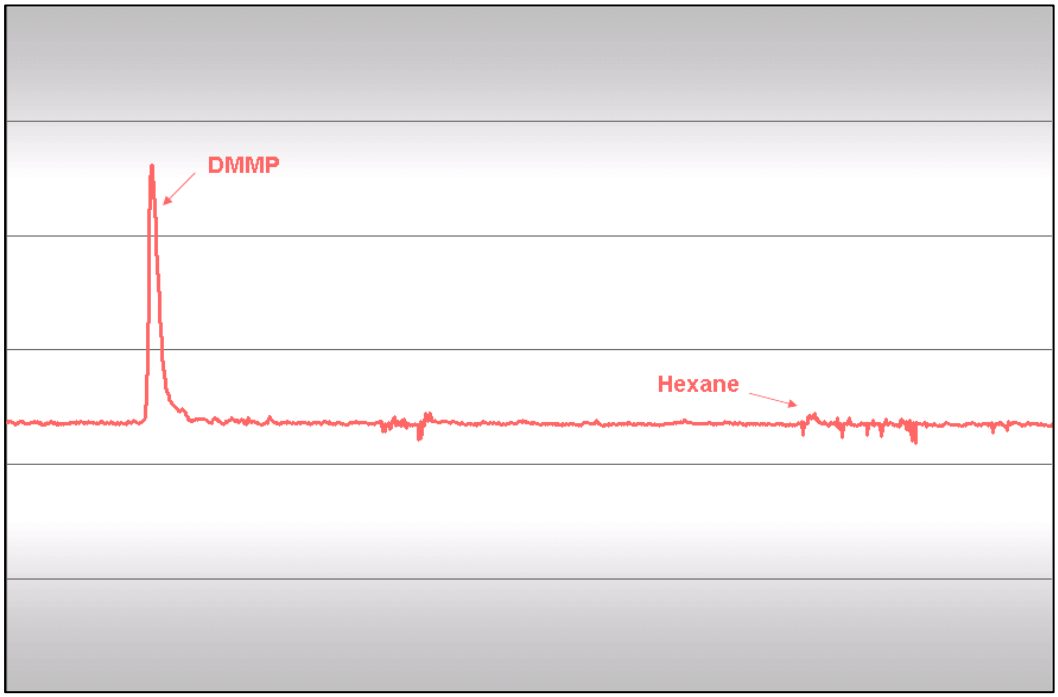

Figure 21: microNPD response showing excellent response to a phosphorous compound but minor response to hexane.

8. FPD

The modifications of Figure 13 were used to allow optical detection of the relaxation of analyte compounds excited in the flame zone of the microcombustor. As noted above, an optical fiber was used to remotely interrogate the flame zone; a PMT or Geiger photodiode was coupled to the fiber with an intermediate notch filter. For sulfur detection a 394 nm filter was used, for example. Detection of peaks of 40 ppm of H_2S is shown in Figure 22. The baseline shift due to 40 ppm injection of CS_2 is shown in Figure 23.

Initial studies into the optimum location of the fiber were undertaken. A top-down approach was beneficial to preventing soot from gradually obscuring the sensor performance. However, given the flow rates in the system and the fact that decay times are of the order of 10 msec for sulfur compounds, the peak in optical emission can occur as much as 1 cm downstream from the combustion zone. This is actually beneficial, as heat shield requirements diminish, allowing the detector to be placed closer to the outlet tube without need for a fiber, enhancing response. This improvement will be undertaken next.

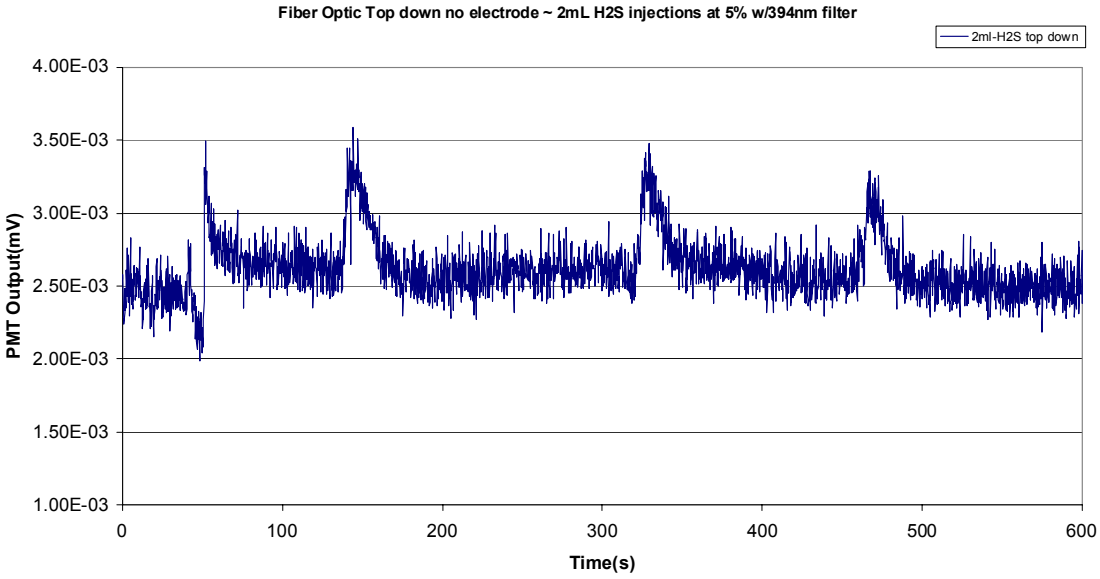

Figure 22: MicroFPD response to injections of 40 ppm of hydrogen sulfide.

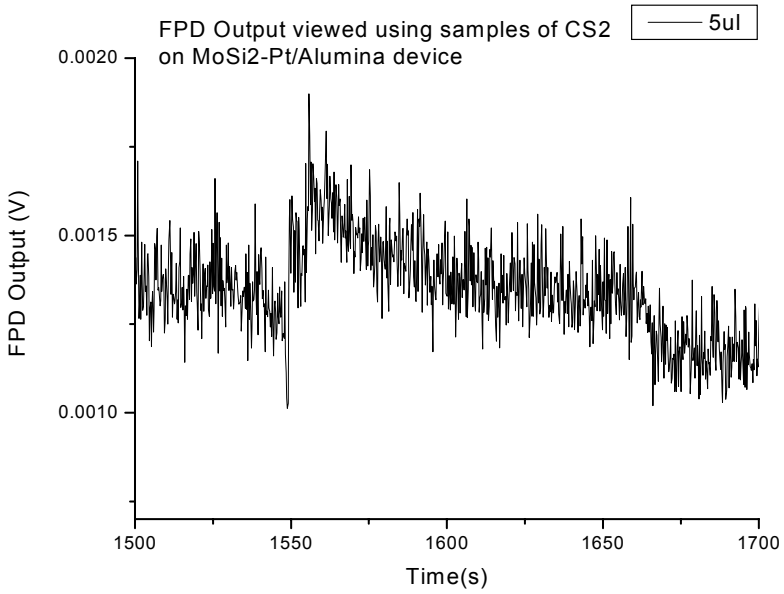

Figure 23: Response of the microFPD to a 40 ppm carbon disulfide injection.

9. Combined detection

The data of **Error! Reference source not found.** and **Error! Reference source not found.** were actually taken with the constant-resistance control circuit functioning as the hotplate heater. That is, the circuit of Figure 14 replaced the simple power supply listed as "heater" in Figure 5. Simultaneous microFID and calorimetry signals were obtained in this manner. Figure 24 illustrates the dual response, which for the compounds shown is simply confirmatory: both devices respond simultaneously to the hydrocarbons shown. However, for CS_2, which yields both calorimetry and optical responses, there is no detectible ion peak. This type of analysis provides speciation. Simultaneous microFPD and calorimetry is shown in figure… Note, simultaneous microNPD and calorimetry could also be performed, allowing calorimetric detection of all species and NPD detection of only compounds containing these elements. This work shows how two microcombustor platforms, one with a catalyst and one with a low work function material, can be used to achieve simultaneous calorimetry, microFID, microFPD and microNPD. The addition of one more inactive microcombustor would allow cancellation of common-mode effects such as ambient temperature and flow variations. Thus a two or three element array of microcombustors would provide a wide array response from a general response to hydrocarbons to specific detection of N, P, S, As containing compounds.

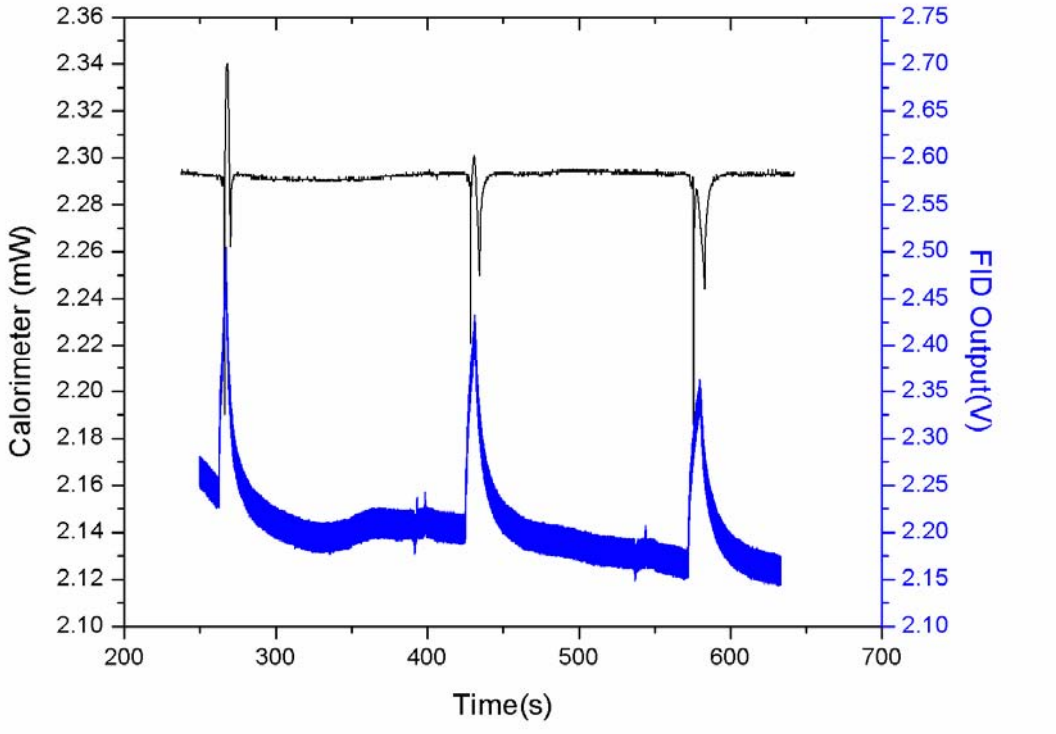

Figure 24: Dual calorimetry and microFID responses.

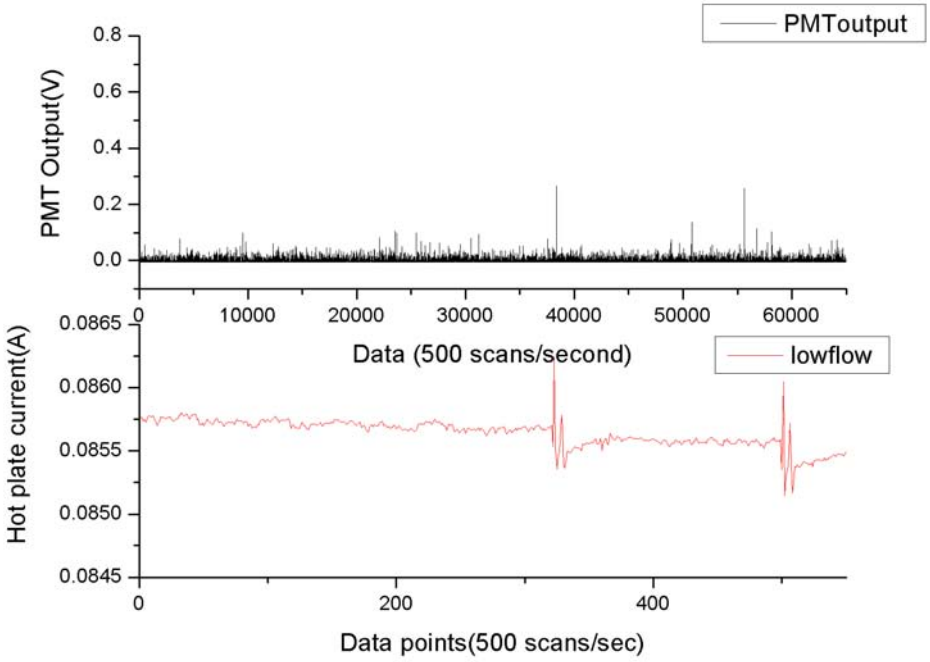

Figure 25: Dual calorimetry and microFPD resonse to hydrogen sulfide injections.

10. Miscellaneous

Reference 15 was the result of this project and several more articles are in preparation: two conference proceedings and one journal article. The microcombustor has been patented (US Patent 6,786,716) and several disclosures have been placed. Funding from various sources is now being pursued to allow advancements on the technology.

11. Conclusions

By placing electrodes and optical detectors around the flame zone of a microcombustor, a microFID, microNPD and microFPD have been constructed and demonstrated. With a minimum of two such microcombustors, one with a catalyst to generate a flame and one with a low-work-function material to generate a NPD, simultaneous FID, NPD, FPD and calorimetry can be performed. The addition of one more inactive microcombustor would allow cancellation of common-mode effects such as ambient temperature and flow variations. Thus a two or three element array of microcombustors would provide a wide variety of response from general hydrocarbon detection to specific detection of N, P, and S compounds. This is important since high selectivity can be obtained with a device having a footprint about the size of a quarter, packaging included. Low hydrogen use and power consumption of this device make it amenable to portable use, and the selectivity of the array will allow it to perform well in the real world. This is especially true if combined with a microGC to perform field separations. Future work will in fact concentrate on optimization for field use and complete testing of the monolithically-integrated collection electronics introduced herein. The various modes of detection of this platform will allow application to several important areas including homeland security, sulfur detection and petrochemicals.

12. References

[1] H. H. Hill and D. G. McMinn, Detectors for Capillary Chromatography, Wiley, 1992, p7.
[2] T. Holm, Aspects of the mechanism of the flame ionization detector, J. Chromatography A, 842 (1999) 221-227.
[3] D.K. Bohme, Kinetics of Ion-Molecule Reactions, P.J. Ausloss, Ed., Plenum Press, NY, 1979.
[4] H.F. Calcote, 8th Int. Symp. Combust. (1962) 184.
[5] J. Deckers, A. van Tiggelen, Combust. Flame 1 (1957) 281.
[6] P.F. Knewstubb, T. M. Sugden, Proc. Royal Soc. London Ser. A 225 (1960) 520.
[7] S. Zimmermann, S. Wischhusen, J. Muller, Micro flame ionization detector and micro flame spectrometer, *Sensors And Actuators B,* 63 (2000) 159-166.
[8] S. Zimmermann, P. Krippner, A. Vogel and J. Muller, Miniaturized flame ionization detector for gas chromatography, *Sensors And Actuators B,* 83 (2002) 285-289.
[9] R. Srinivasan, I-M Hsing, J. Ryley, M.P. Harold, K.F. Jensen, and M.A. Schmidt, Micromachined chemical reactors for surface catalyzed oxidation reactions, *Tech. Digest 1996 Sol.-State Sensor and Actuator Workshop*, Transducers Research Foundation, Cleveland (1996) 15-18.
[10] L. R. Arana, S.B. Schaevitz, A.J. Franz, K.F. Jensen and M.A. Schmidt, A microfabricated suspended-tube chemical reactor for fuel processing, MEMS 2002, Las Vegas, NV, 1/20-24/2002, 232-235.
[11] M. Gall, The Si-planar-pellistor array, a detection unit for combustible gases, *Sensors and Actuators B*, 15-16 (1993) 260-264.
[12] R.P. Manginell, J.H. Smith, A.J. Ricco, D.J. Moreno, R.C. Hughes, R.J. Huber and S.D. Senturia, Selective, pulsed CVD of platinum on microfilament gas sensors, *Tech. Digest 1996 Sol.-State Sensor and Actuator Workshop*, Transducers Research Foundation, Cleveland (1996) 23-27.
[13] R.E.Cavicchi, J.S. Suehle, P. Chaparala, K.G. Kreider, M. Gaitan, and S. Semancik, Micro-hotplate gas sensor, *Tech. Digest 1994 Sol.-State Sensor and Actuator Workshop*, Cleveland (1994) 53-56.
[14] M.Zanini, J.H.Visser,L.Rimai,R.E.Soltis, A.Kovalchuk,D.W.Hoffmann, E.M. Logothetis, U. Bonne, L. Brewer, O.W. Byrnum, M.A. Richard, Fabrication and properties of a Si-based high sensitivitiy microcalorimetric gas sensor, *Tech. Digest 1994 Sol.-State Sensor and Actuator Workshop*, Cleveland (1994) 176-179.
[15] M. Moorman, R. P. Manginell, C. Colburn, D. Mowery-Evans, P. G. Clem, N. Bell, and L. F. Anderson, Microcombustor Array and Micro Flame Ionization Detector for Hydrocarbon Detection, Proc. SPIE, 4981 (2002) 41-50.
[16] S.L. Firebaugh, K.F. Jensen, M.A. Schmidt, Investigation of high-temperature degradation of platinum films with an in situ resistance measurement apparatus, *Journal Of Microelectromechanical Systems ,* 7 (1998) 128-135.
[17] D. Briand, S. Heimgartner, M. Leboeuf, M. Dadras and N.F. de Rooij, Processing influence on the reliability of platinum thin films for MEMS applications, *MRS Symposium Proceedings*, 729 (2002) 63-68.
[18] R.P. Manginell, J.H. Smith, A.J. Ricco, D.J. Moreno, R.C. Hughes, R.J. Huber, "Electro-thermal modeling of a microbridge gas sensor", SPIE's 1997 Symposium on Micromachining and Microfabrication, Austin, TX, Sept. 29-30, 1997. SPIE Vol. 3224, pp. 360-371.
[19] J. Thornton, D. Straub, G. A. Richards, R. S. Nutter Jr., E. Robey, An in-situ monitoring technique for control and diagnostics of natural gas combustion systems, The 2nd Joint Meeting of the U.S. Sections of the Combustion Institute, Oakland, CA. March 25-28, 2001.
[20] N. G. Norton, E D. Wetzel and D. G. Vlachos, Fabrication of single-channel catalytic microburners: effect of confinement on the oxidation of hydrogen/air mixtures, Ind. Eng. Chem. Res, 2004, 43 4833-4840.

Distribution:

1	MS0892	Thomas Hamilton	1722
1	MS0892	Patrick Lewis	1722
2	MS0892	Ron Manginell	1722
1	MS0892	Matthew Moorman	1722
1	MS0892	Cody Washburn	1722
1	MS1080	Murat Okandan	1080
1	MS1349	James Miller	1349
1	MS1411	Paul Clem	1349
2	MS9018	Central Technical Files	8945-1
2	MS0899	Technical Library	9616
1	MS0188	D. Chavez, LDRD Office	1030
1	MS0161	Patent and Licensing Office	11500